

WFPC2 Flatfields with Reduced Noise and an Anomaly of Filter FQCH4N-D

E. Karkoschka

Lunar and Planetary Lab, University of Arizona, Tucson, AZ 85721

A. Koekemoer

Space Telescope Science Institute, 3700 San Martin Drive, Baltimore, MD 21218

Abstract. The transmission of the filter FQCH4N-D varies by 20 percent across the filter while the mean wavelength shifts by 3 nm. For objects with a flat spectrum across the main bandpass (889–897 nm), the flatfielding removes the spatial variations except for the outer corner, for which we give the necessary photometric correction. On the other hand, for objects with steep spectral features within the bandpass, such as Jupiter and Saturn, the spectral shift causes photometric variations of some 30 percent across the filter which are not taken out by flatfielding. We give the magnitude and direction of the shift to account for these variations. Flatfields with reduced noise are described in the *Instrument Science Report* WFPC2 2001-07 http://www.stsci.edu/instruments/wfpc2/Wfpc2_isr/wfpc2_isr0107.html and not repeated here, except for the abstract: We examine the noise contributed by the WFPC2 flatfields during normal calibration, and provide new low-noise flats for 41 filters. Highly exposed science images (> 20,000 electrons per pixel) will show significant noise reduction if these new flats are used; this is especially true for images on the PC1 chip. For some ultraviolet filters a significant improvement occurs even for much lower exposure levels. Potential photometric issues are also discussed. The new flats are available in the *HST* data archive as calibrated science data (i.e., data which have already calibrated with the normal flatfields) to obtain the noise reduction. These corrections may be incorporated in the normal pipeline flatfields at some future date for selected filters.

1. Introduction

The filter FQCH4N of WFPC2 is a quad filter which selects narrow bandwidths in four methane absorption bands. This gives unique vertical probing of planetary atmospheres and reduces stray light from planets when imaging nearby rings or satellites. Therefore, this filter has been the filter most often used for planetary imaging. Eighty percent of the observations with the filter FQCH4N use the quad with the deepest methane absorption, the filter FQCH4N-D, which is the focus of this study.

In 1994, we found that images of Jupiter in the filter FQCH4N-D could not be modeled, unlike many other observations. The images showed an unexplained discrepancy of about 30 percent intensity between the east and west limb of Jupiter. On the other hand, Galilean satellites had consistent counts across the field of view. We concluded that the filter has a spatial change of the spectral response which affects the photometry of objects depending on their spectrum. A warning of a possible spatial variation was posted on the WFPC2 web site at http://www.stsci.edu/instruments/wfpc2/Wfpc2_phot/wfpc2_phot/wfpc2_phot0107.html

Another indication that this filter is unusual is documented in its flatfield displaying an anomalous brightness variation of 30 percent with respect to other filters at similar wavelengths. Flatfield variations between different filters of similar wavelengths are typically on the order of one or a few percent; a variation of 30 percent is only present with one other WFPC2 filter, which is FQCH4N-

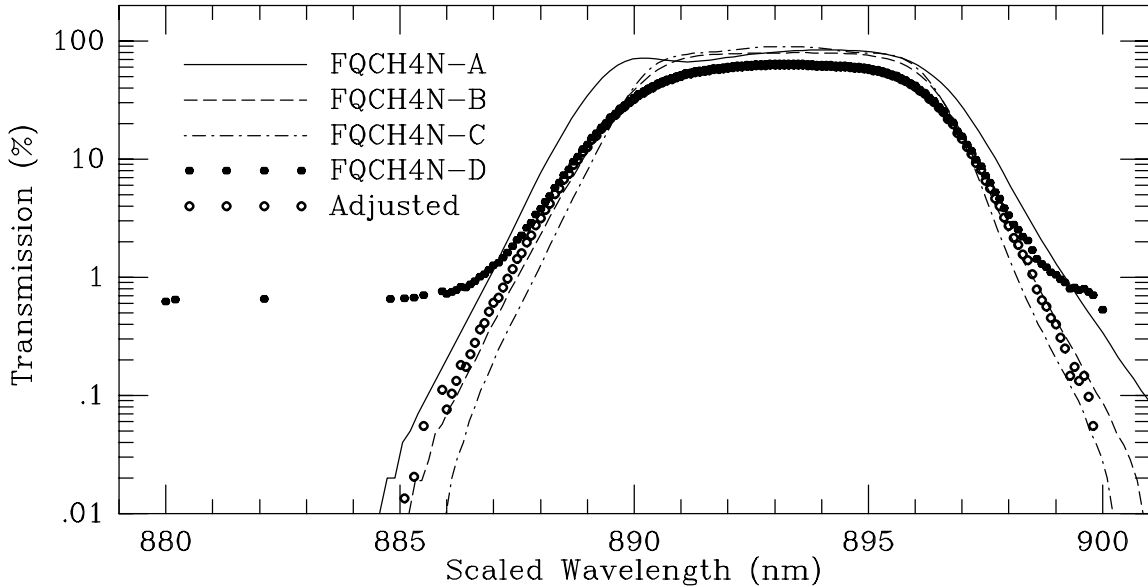


Figure 1. Transmission curves for the four methane quad filters with the wavelengths scaled to the same mean. For FQCH4N-D, the original and adjusted transmission curves are shown.

C. While this filter could have similar problems as FQCH4N-D, an investigation of its properties would benefit very few programs because of the low usage of FQCH4N-C.

In September, 2001, one orbit was devoted to characterize the spatial variation of filter FQCH4N-D. Nine images of Saturn were taken with identical exposure times but with different locations covering the whole unvignetted field of view. The rings of Saturn yielded consistent photometry across most of the field of view as expected since they have similar spectra as the Galilean satellites. Counts on Saturn's globe showed a photometric discrepancy of about 25 percent across the field of view as expected since Saturn's globe has a similar spectrum as Jupiter. We use these observations to characterize the filter FQCH4N-D.

Before we describe the observations further in Section 4, we look at the basic calibration data of the filter, its spectral transmission measurements (Section 2) and its flatfield (Section 3). Section 5 describes the usable field of view. Section 6 gives a recommended adjustment to the flatfield. Section 7 explains the observed photometric discrepancy. The last section concludes with summarizing suggestions for users of the filter FQCH4N-D.

2. Spectral Transmission Curve

The measured spectral response curve of the filter FQCH4N-D is available at the WFPC2 web site: http://www.stsci.edu/instruments/wfpc2/Wfpc2_thru/fqch4nd.txt. It is plotted in Figure 1 along with the transmission curves of the other three methane quad filters, which have been scaled in wavelength to allow the comparison. For transmission values above 1 percent, all four curves have a similar shape. However, for the scan between 880 and 900 nm, the low transmission numbers of the filter FQCH4N-D seem to level off near 0.65 percent without decreasing any further. This is unlike the other three filters which plunge steeply below 0.01 percent transmission. We assume that the leveling off at 0.0065 transmission for the FQCH4N-D filter is not real but an artifact of the measurement, such as a constant contribution from background light. We adjust the transmission values of the filter FQCH4N-D by subtracting 0.0065 of each value whenever the original value is higher and setting it to zero otherwise. This is the adopted transmission, shown by the open circles in Figure 1. It follows the shape of the other three curves quite well.

The original transmission curve has a higher integrated throughput than the adjusted one. For objects with a flat spectrum, the increase is 8 percent. For objects with methane absorption, the increase is estimated at 38, 34, 14, 21, and 17 percent for Jupiter, Saturn, Titan, Uranus, and Neptune, respectively, based on published spectra (Karkoschka 1998). Thus, this adjustment yields a very significant photometric correction.

3. The FQCH4N-D Flatfield

Figure 2 (top left) displays the flatfield of FQCH4N on WF3 divided by the flatfield of F850LP which has a similar mean wavelength as FQCH4N-D. Note that the flatfield is displayed here in brightness units while STScI flatfields are usually given in inverse brightness so that they can be multiplied into the raw image. Obvious are the curved edges near the center and the bottom right where light through the FQCH4N-D quad is vignetted and light through the FQCH4N-C and FQCH4N-A filters, respectively, starts to contribute.

Inside the unvignetted field of view, the brightness increases from the bottom to the upper right. A least-square fit to the data gives a gradient direction of 37 degrees counterclockwise from horizontal. In the perpendicular direction, the brightness scatters by only one percent or less (Figure 3). Thus, the observed spatial variation is a function of only one variable, plotted on the x -axis of Figure 3. We chose the center of the WFPC2 pyramid as the origin of this axis.

Figure 3 also displays another ratio of two flatfields of similar mean wavelengths, F785LP and F850LP. In this case, the ratio remains close to unity throughout the field of view. Other ratios behave similarly. The strange slope of FQCH4N-D cannot be due to variations in spectral sensitivity of pixels. It is due to a spatial variation in the transmission properties of the filter.

4. Image Processing

The nine images of Saturn taken for this program were processed with the standard WFPC2 calibration pipeline. Then, a total of 777 pixels were identified which had elevated counts, mostly due to cosmic ray strikes. The flatfielded counts of those pixels were replaced by counts interpolated from pixels outside the contaminated areas. The filter FQCH4N-D was used in its rotation FQCH4N, where it extends mostly across the WF3 chip. Its small section on the WF2 chip did not produce data suitable for photometry. Figure 2 (top right) shows the nine calibrated images laid on top of each other, with the maximum data number at each pixel displayed.

The next image processing step was image navigation, which was performed for each of the nine images to an accuracy of about 0.05 pixels, taking into account the distortion for the WF3 chip. After the relative offsets of Saturn in the nine images were determined, the nine coordinate pairs for a location on Saturn can be calculated. This calculation was performed for some 100,000 locations. The interpolation of data numbers to fractional pixels used the 64 pixels of the 8×8 -pixel box centered on the fractional pixel with cubic interpolation in both axes.

A mean image of Saturn was created by averaging the nine images accounting for the appropriate offsets. At each location, the weighting for the averaging was largest for pixels in the center of the field of view and zero outside the unvignetted field of view (described in Section 5). The weighting function was the product of the distances to the edges of the unvignetted field of view.

Each of the nine images was divided by the shifted mean image. In a perfect world, all divided images should have data numbers of unity. Deviations from unity show various imperfections (Figure 2, bottom). First, we note that vignetted regions do not divide out well at all. We need to restrict ourselves to the unvignetted part of the field of view, described in Section 5. Second, the rings seem to perform close to perfect, except for the upper right-hand corner where data numbers drop, which is investigated in Section 6. Third, Saturn's globe is brightest in the bottom images and faintest in the upper right-hand images, which is investigated in Section 7. Fourth, the division is not perfect at sharp edges of the planet. This is probably due to imperfections in the knowledge of the distortion.

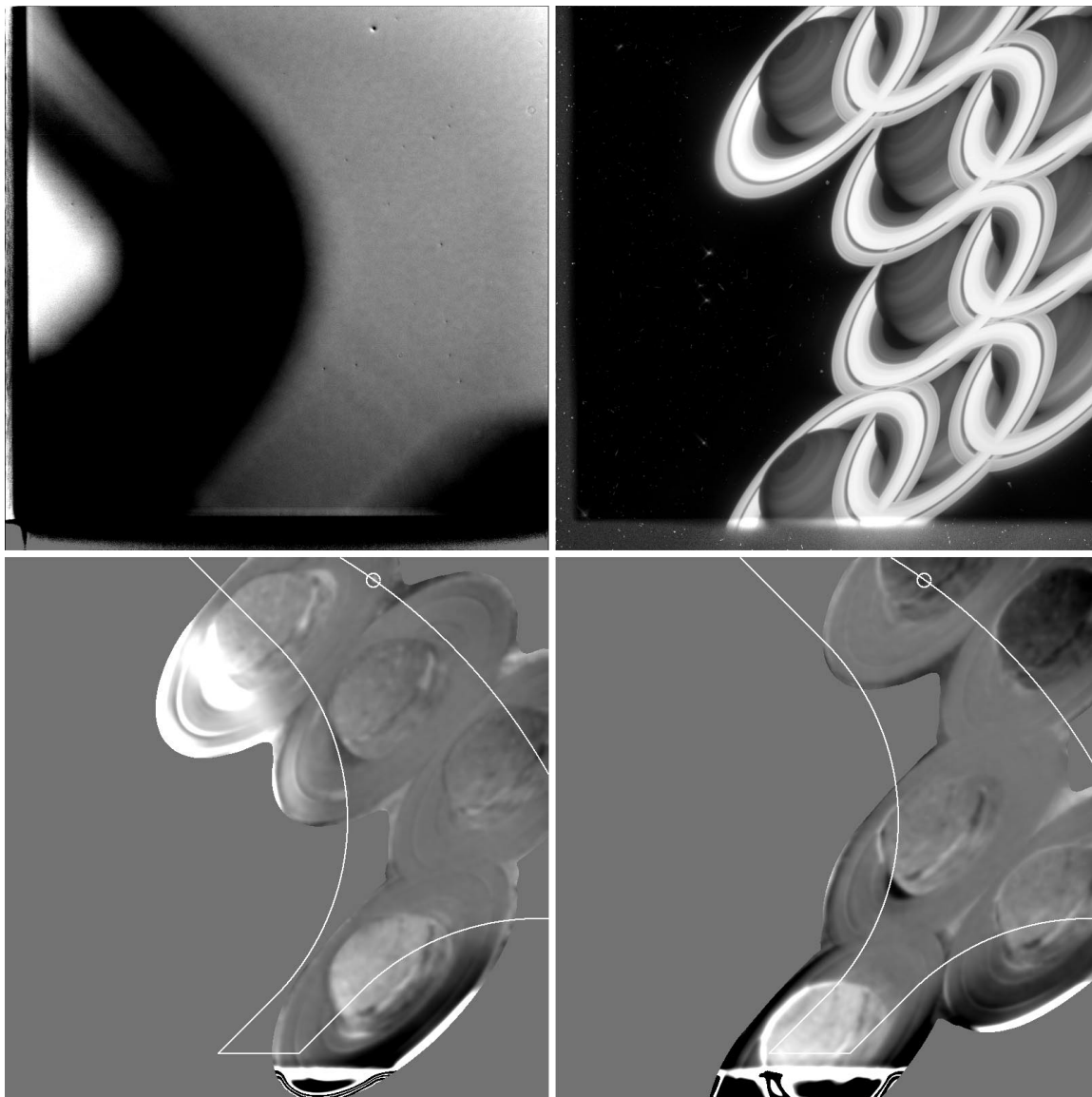


Figure 2. *Top left:* Ratio of the flatfield brightness of FQCH4N-D/F850LP. *Top right:* Nine overlaid flatfielded images of Saturn in FQCH4N-D on WF3. *Bottom:* The same nine images after division by the mean image of Saturn. To avoid cluttering, images are shown either on the left or on the right side. The white lines mark the adopted edge of the unvignetted field of view.

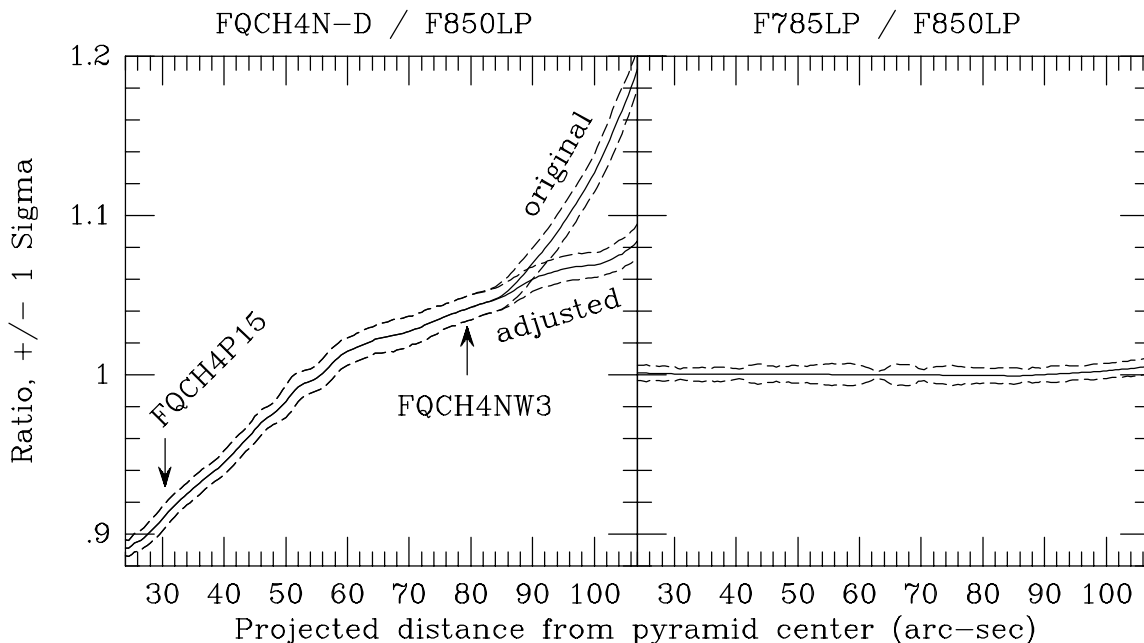


Figure 3. Flatfield brightness ratios on WF3 for FQCH4N-D (left) and F785LP (right) relative to F850LP. The spatial variable is the x -coordinate in a coordinate system rotated 37 degrees counterclockwise from the WF3 system with the pyramid center as the origin (column 30, row 47 of WF3).

Therefore, we discard data within three pixels of those edges, which leaves more than 90 percent of the data. Finally, we note a bright latitudinal feature just south of Saturn's equator. Since it rotates during the time period of the nine exposures, it does not divide out. Therefore, we exclude this latitude zone from our analysis. No other longitudinal features are obvious on Saturn. However, a close investigation of divided images yields more features of low contrast, typically 1–2 percent. Thus, results on Saturn's globe will be limited to that accuracy.

5. Vignetting

For the determination of the edges of the usable field of view, we use Saturn's rings and exclude locations within three pixels of Saturn's globe. We distinguish five edges (cf. Figure 2, top left): the rounded edge near the center towards the quad FQCH4N-C, the horizontal edge at the bottom towards WF2, the rounded edge at the bottom right towards the quad FQCH4N-A, the right edge of WF3, and its top edge.

We define the usable field of view as the area where the divided ring counts are within about one percent of unity, which means that photometry is consistent to one percent across this area. Figure 4 (left) displays the mean deviation of counts from unity in the divided ring images as a function of distance from the adopted locations of the edges. According to Figure 4, photometric errors rise quickly above several percent outside the adopted edges, where an image might be still useful for feature recognition, but not for photometry. Furthermore, a spot of 10 pixel radius around pixel (543,767) does not flatfield out. It is visible on the left side of Figure 2, near the very top.

For the rotation FQCH4P15 of the filter FQCH4N-D, we estimated the shift and used the rotation of 15 degrees to derive its unvignetted field on PC1. The adopted unvignetted fields are displayed in Figure 5. Its definition for WF3 is: $|y - 677| > 397 - x$ and $\sqrt{(x - 135)^2 + (y - 415)^2} > 370$ and $|y - 153| > 397 - x$ and $y > 72$ and $|x - 523| > 162 - y$ and $\sqrt{(x - 785)^2 + (y + 100)^2} >$

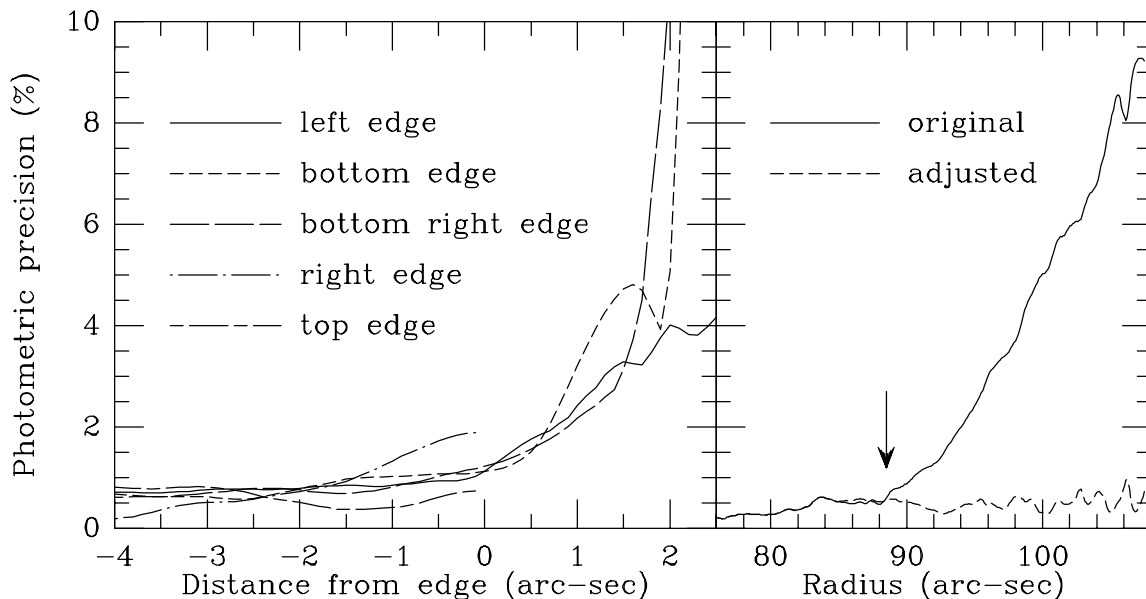


Figure 4. Deviation of divided ring counts from unity for FQCH4N on WF3, displayed as function of distance from the adopted edges of the unvignetted field of view (left), and displayed as function of radius from the pyramid center for the original and adjusted flatfield (right). The arrow corresponds to the dashed line in Figure 5.

370 and $x < 800$ (or $x < 790$ for higher precision) and $y < 800$, and $\sqrt{(x - 543)^2 + (y - 767)^2} > 10$. The definition for PC1 is: $y > 100$ and $y > 1.73x - 623$ and $y < 665 - 0.58x$ and $y < 1.73x - 258$ (x is the column number and y is the row number).

6. Flatfield Imperfection

Figure 4 (right) displays divided ring counts near the upper right-hand corner of WF3. Starting near a radius of $r = 88.5$ arc-seconds from the center of the pyramid ($x = 30$ and $y = 47$), the ring counts deviate by up to nine percent from unity. However, by multiplying ring counts by $1 + 2 \times 10^{-6}(r - 84)^2$, all counts are brought back to unity within the typical scatter. We think that the upper right-hand corner of WF3 can be used photometrically after applying the given correction. The decrease of ring counts near that corner seems to derive from excess light in the flatfield (Figure 3). Thus, the best way to correct this defect is a change in the flatfield of FQCH4N on WF3. With this correction, the average deviation of divided ring counts from unity inside the unvignetted field of view is 0.4 percent. Thus, the filter is suitable for excellent photometry.

7. Spectral Shift

We divide Saturn into three sections: the rings and both latitude regions south and north of the latitude zone with the obvious longitudinal feature. Again, locations within three pixels of a boundary are excluded from all sections. Counts of divided images vary systematically by 2, 30, and 20 percent across the field of view for the rings, southern latitudes, and the Equatorial Zone, respectively. Least-square fits to both variations on Saturn's globe yield gradient directions near 37 degrees counterclockwise from the x -axis of WF3, the same as for the flatfield variation discussed in Section 3. Thus, in Figure 6 we plot the divided counts as functions of the same variable used for Figure 3.

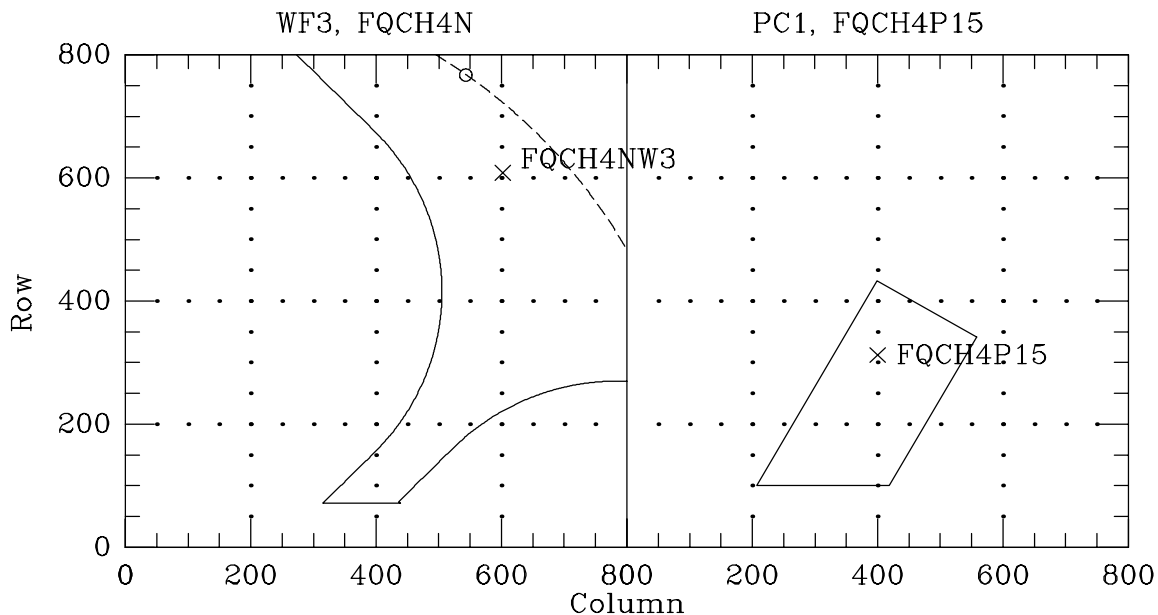


Figure 5. Outlines of the unvignetted fields of view for the filter rotation FQCH4N on WF3 and FQCH4P15 on PC1. The area outside the dashed line requires a flatfield correction.

Most likely, the filter FQCH4N-D has a spatial variation such as a variation in the thickness of a layer. This causes the variation in the flatfield (Section 3) as well as the different variations seen in Figure 6. While the flatfield variation can be explained by transmission values changing in the same way for all wavelengths, the variation seen in Figure 6 requires a spectral variation. The easiest explanation is a spectral shift of the whole transmission curve.

A small spectral shift can cause the observed variations since Saturn displays steep spectral features within the bandpass of FQCH4N-D (Figure 7). Notably, from the short wavelength end of the filter's passband to its opposite end, Saturn's flux increases by a factor of two or more.

We assume that the transmission curve of the filter FQCH4N-D was measured at the aperture FQCH4NW3, that it is shifted by 2 nm longward at the aperture FQCH4P15, and that the shift is linear and in the direction 37 degrees counterclockwise from the horizontal axis of WF3. This assumption can explain the approximate size of the variations seen for both sections of Saturn's globe (curves in Figure 6). It also explains the approximate shape of the variations. The fact that the curves do not match the dots perfectly may result from observational limitations such as rotating longitudinal features on Saturn or spectral variations within each of the two selected sections. In view of these limitations, better fits possible with a more sophisticated dependency of the spectral shift as function of location seem unwarranted.

Based on the relative flatfield brightness of the four methane quads, we estimate that the flatfield source had a color temperature near 3000 K. The spectrum of the ring is close to a solar spectrum with a color temperature near 6000 K. This difference causes a slight variation of flatfielded ring counts across the field of view which is even hinted at by the data, the slightly sloping data points for the rings in Figure 6.

The adopted shift at each pixel can be calculated by $(602 - x)0.0032 \text{ nm} + (608 - y)0.0024 \text{ nm}$ for the rotation FQCH4N on WF3 and $2 \text{ nm} + (x - 400)0.0011 \text{ nm} + (y - 312)0.0014 \text{ nm}$ for the rotation FQCH4P15 on PC1. The total wavelength shift across the whole unvignetted field of view of the filter FQCH4N-D is 3.3 nm. This shift causes brightness variations across the filter FQCH4N-D of factors of 1.29, 1.24, 1.05, 1.01, and 1.02 for Jupiter, Saturn, Titan, Uranus, and Neptune, respectively based on spectra by Karkoschka (1998). However, spectral variations across

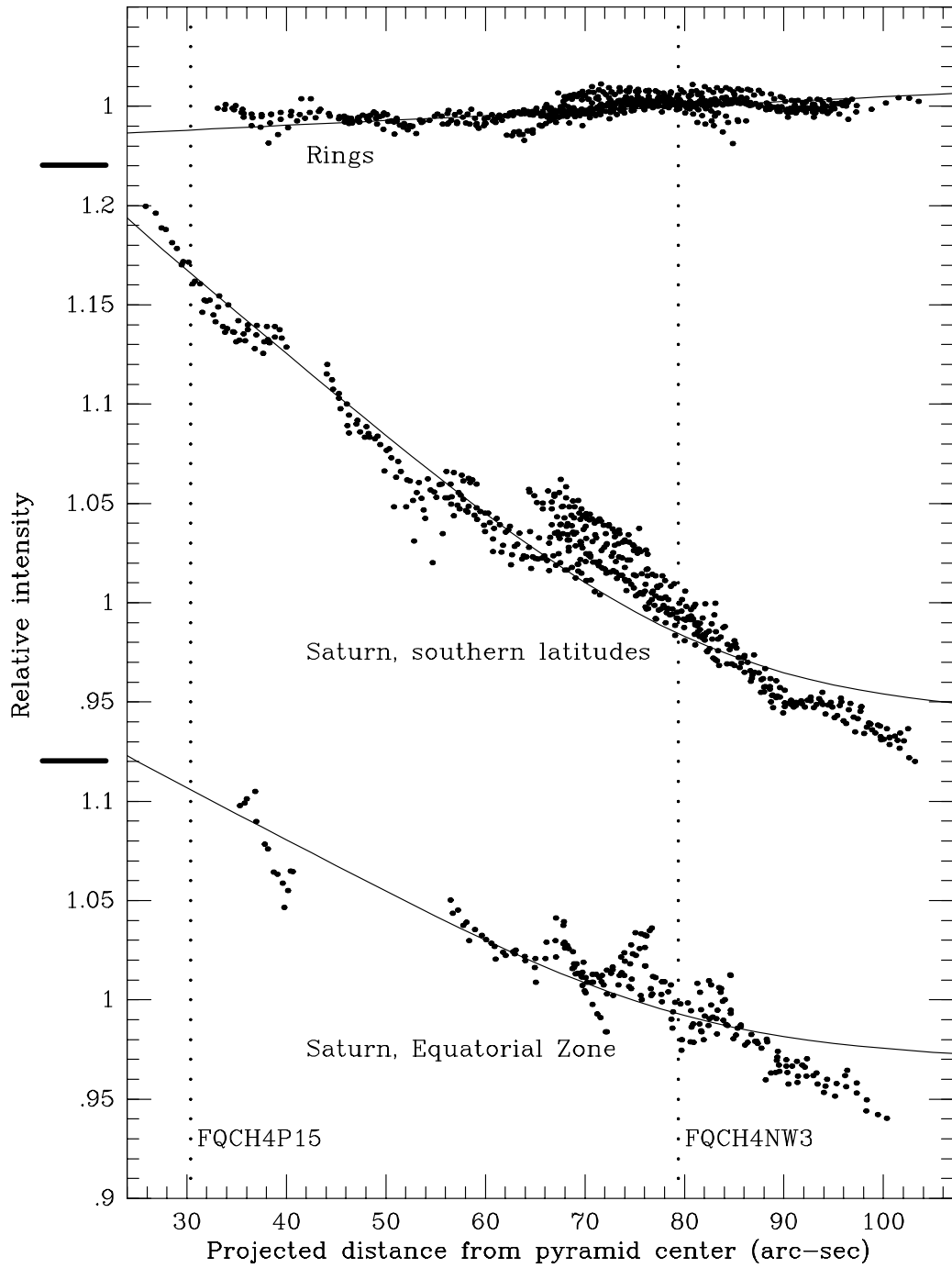


Figure 6. Divided counts on three parts of Saturn as function of location (dots). The curves are the expected variations for the adopted wavelength shift of the filter FQCH4N-D.

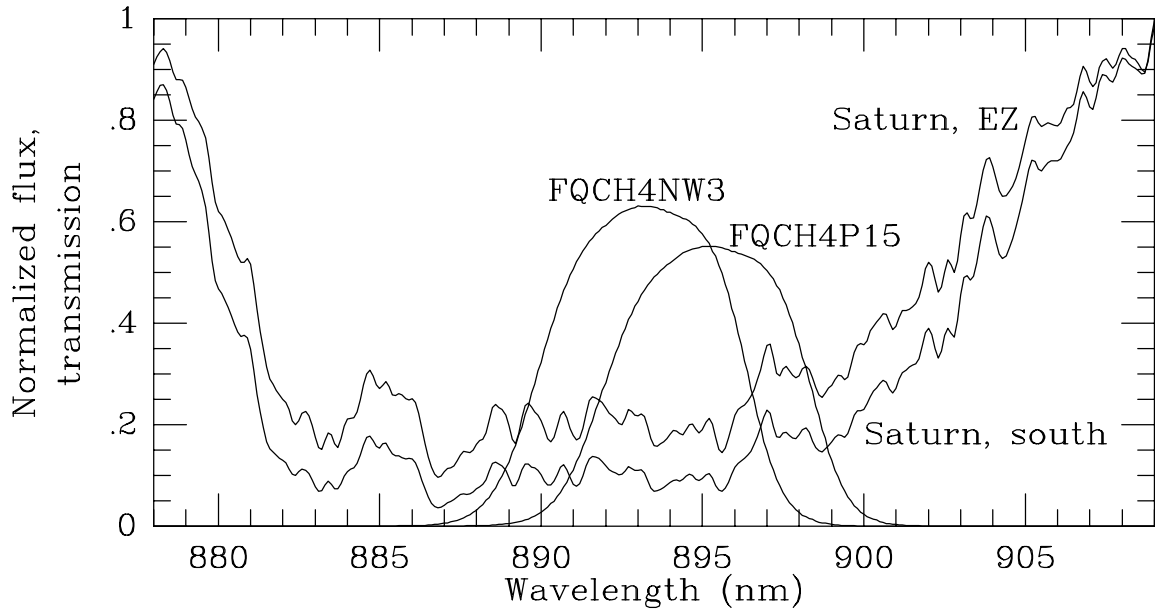


Figure 7. Adopted filter transmission curves for two apertures and the spectra of two regions on Saturn, taken from the same observations as published by Karkoschka (1998).

each planetary disk are significant so that these averages are only a rough guide for actual variations of specific features on each disk.

8. Recommendations

1. An object should be placed inside the unvignetted field of view, shown in Figure 5. For the WF3, a placement towards the upper right yields higher signals due to the higher transmission of the filter.
2. A placement outside the dashed line of Figure 5 is only recommended if necessary because of some uncertainty of the flatfield adjustment.
3. The flatfield of FQCH4N-D in rotation FQCH4N on WF3 should be adjusted according to Section 6.
4. The transmission values of filter FQCH4N-D should be reduced by 0.0065 according to Section 2.
5. The transmission curve of FQCH4N-D should be spectrally shifted as explained in Section 7. This shift is most important for photometry on Jupiter and Saturn.
6. The observations of Saturn for this work gave a guide to understand the characteristics of filter FQCH4N-D, but they cannot replace measurements of the filter transmission curve at various locations of the filter. While this was not done before the installation of WFPC2 on *HST*, it may be possible to do when WFPC2 is brought back to the ground.
7. Other WFPC2 filters such as F953N also have anomalous brightness variations of the flatfield and measured transmission values which do not seem to reach zero. While they are smaller than those of FQCH4N-D, they still may be significant for some applications.
8. Measurements of filter transmission curves are preferentially performed at several locations since some filters are not spatially homogeneous.

References

Karkoschka, E. 1998, *Icarus*, 133, 134